Supplement: Modeling actinic flux and photolysis frequencies in dense biomass burning plumes

Correspondence: Jan-Lukas Tirpitz (jltirpitz@atmos.ucla.edu)

S1 Parameterisation of wavelength-dependencies

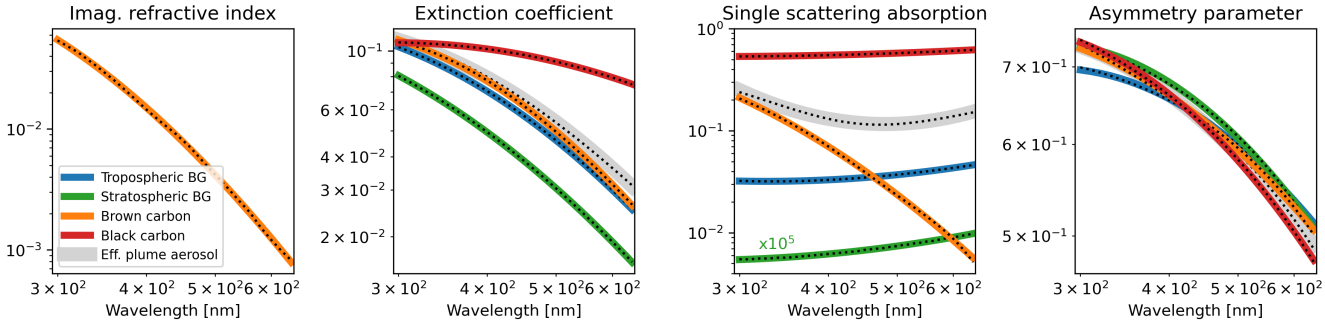

Figure S1. Parameterisation of the wavelength-dependence of various parameters based on Eq. 4. The single scattering co-albedo is defined as 1-SSA (see Section 2.5). For detailed description and discussion, see text.

This Supplement demonstrates the applicability of Eq. 4, which we propose in Section 2.5 as a general parameterisation approach for wavelength-dependent parameters. Each panel in Figure S1 shows another wavelength-dependent parameter, as indicated by the panel titles. Black dots in Figure S1 represent ground truths, based on measurements performed during plume transect 5 (see also Figure 5). For ground truth values of the brown carbon imaginary refractive index (left panel), we use the wavelength-dependence measured by the SAEB instrument (see Section 3.2) and a magnitude retrieved as described in Section 4.2. Ground truths for extinction coefficient, single scattering absorption and asymmetry parameter were calculated with the Mie model, assuming aerosol microphysical properties as described in Section 4. From the particle refractive indices used in this study (see Section 4), only the brown carbon imaginary refractive index features a significant and well-known wavelength-dependence; thus it is the only refractive index shown here. We fit the proposed parameterisation (Eq. 4) to the to the ground truth data. The fit results are indicated by the colored lines. Different colors indicate different aerosol types (see legend), as specified in more detail in Section 4. Thick light-grey lines show "effective plume aerosol", representing the combined bulk optical properties of black and brown carbon, assuming the transect 5 optical black carbon fraction (see Section 4.2 for its definition). Deviations between the ground truth and the fitted curves are barely visible, indicating that Eq. 4 can accurately

describe wavelength-dependencies of various aerosol related parameters and aerosol types, including brown carbon. The order number (i_{max}) used here in Eq. 4 is 3 for the brown carbon imaginary refractive index, and 2 for all other parameters. In general, i_{max} can be adapted to the respective application, depending on the types of aerosol and the acccuracy requirements.

S2 Spectral interpolation

This Section relates to the spectral interpolation approach described in Section 2.5, used to reproduce high resolution spectra from simulations at a limited number of wavelength nodes. Here, we specify the interpolation settings and assess the accuracy of the reconstructed high resolution spectra. The optimization of the settings and the accuracy assessment were achieved as follows:

1. We calculated ground truth high resolution actinic flux spectra line-by-line on a 0.5 nm grid for various scenarios covering a wide range of conditions.

2. The spectral interpolation was applied and optimized to reproduce the same spectra from simulations at a reduced number of wavelengths (wavelength nodes)

For these investigations, we set up a model atmosphere based on the conditions during the *Spectrum 1* observation (see Figure 5) and modified as follows: the ground level was set to 0 m ASL. Simulations were performed with and without an artificial plume of Gaussian shape (center at 2.5 km, vertical FWHM of 500 m, aerosol vertical optical thickness of 4). We found measurement altitude and SZA to be most critical for the stability of the interpolation. Therefore, we performed simulations at SZAs of 10, 20, 30, 40, 50, 55, 60, 65, 70, 72, 74, 76, 78, 80, 81, 82, 83, 84, 85, 86, 87, 88 and $89°$, while we varied altitudes between 0.1 and 10 km. In total, 322 scenarios were simulated. Literature spectra were smoothed prior to simulation by convolution with a Gaussian kernel of 2 nm FWHM (as described in Section 2.5).

Based on the 322 scenarios, we optimized the settings of the spectral interpolation by trial and error. This optimization comprised (i) splitting the spectral range into suitable interpolation intervals, (ii) finding suitable wavelength nodes carrying the required information for a stable fitting of Eq. 7 and (iii) finding suitable polynomial orders n_p, n_λ and n_σ for the model functions (Eq, 7 and 8). We ended up with the 23 wavelength nodes (296, 298, 300, 303, 307, 310, 315, 320, 330, 340, 350, 360, 380, 400, 430, 447, 462, 506, 538, 588, 603, 620 and 640 nm). These nodes are denser in the UV in order to capture the strong brown carbon and O_3 absorption. Where possible, they were chosen to sample minima and maxima of the O_3 differential absorption structures. We split the spectrum into three wavelength intervals interpolated separately: the *UV* range with the strongest O_3 absorption (requiring higher-order polynomials in Eq. 8), the *UV-Vis* and the *Vis* interval. Spectral range, number of nodes and applied polynomial orders for each interval are listed in Table S1.

Figure S2 summarizes the results. The left panel shows actinic flux spectra for four example scenarios (altitude of 2 km above ground, with and without plume, high and low SZA). In this panel deviations between the exact line-by-line calculations (black) and the reconstructed spectra (blue) are too small to be visible. The right panel shows relative deviations for SZAs smaller (top) and larger (bottom) than $70°$. All 322 scenarios are taken into consideration. For the small SZAs, typical deviations are on the

Table S1. Spectral interpolation settings applied in this study.

	UV	UV-Vis	Vis
Range [nm]	298-360	360-462	447-640
Nodes	11	8	6
n_p	2	3	5
n_λ	3	0	0
n_σ	2	0	0

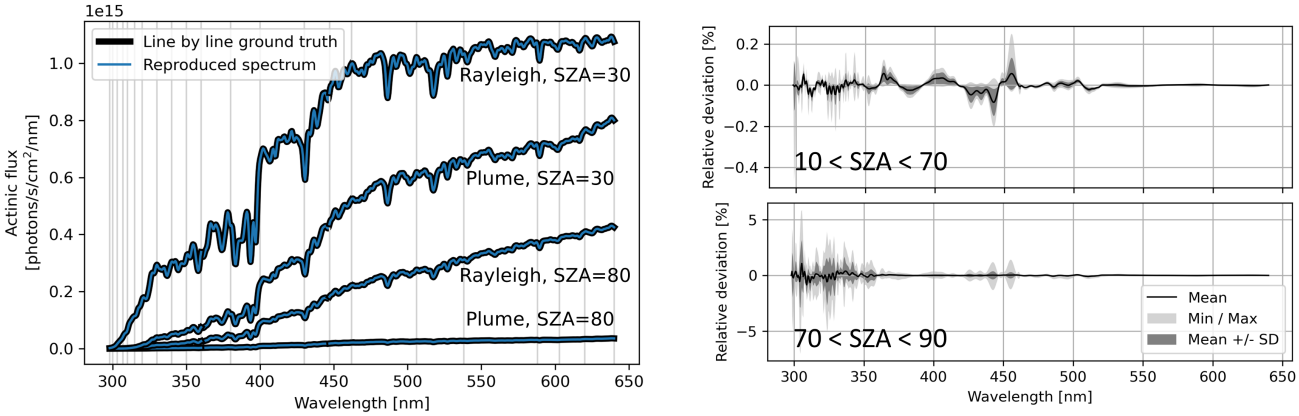

Figure S2. Reconstructed spectra in comparison to exact line-by-line calculated spectra. Left panel shows four example spectra simulated for an altitude of 2 km above ground, with and without plume at high and low SZA. Wavelength nodes used for the spectral reconstruction are indicated by the grey vertical lines. Right panel shows the deviation between reconstructed spectra and exact calculations for two SZA ranges.

order of $0.1\,\%$. For large SZAs, deviations increase to few percent and are highest in the UV. We also calculated photolysis frequencies for the reactions listed in Section S5 from both the exact and the interpolated spectra. Due to the spectral integration inherent in the photolysis frequency calculation process, relative deviations are even smaller here, with an RMS, 99th percentile and maximum of $0.2\,\%$, $1\,\%$ and $1.8\,\%$, respectively.

For final verification we performed a similar study on a subset of spectra from the flight presented in the main text and found deviations in line with the results shown in Figure S2. We conclude that the settings chosen here ensure a stable interpolation with errors negligible compared to other sources of uncertainty, at least for the study presented in the main text.

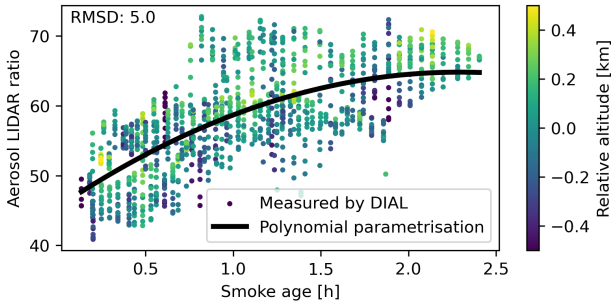

Figure S3. Dependence of the aerosol lidar ratio on smoke age as measured from the lidar during plume overflights. Black line shows the second order polynomial fit for parameterisation. Color-coded is the relative altitude with respect to the plume vertical center of mass.

S3 Parameterisation of the lidar ratio with plume age

The smoke age, i.e. the atmospheric residence time of the sampled smoke, was estimated for each observation by backward integration of wind vectors measured at plume altitude. This relatively simple approach is justified for our study, since smoke ages are primarily used to associate transect and overflight observations from similar parts of the plume (see Section 4.2). It should be noted that the FIREX-AQ dataset includes more accurate smoke age data based on back-trajectory calculations. However, these were only calculated for plume transects, not overflights, and therefore could not be used for our purpose.

S4 Actinic flux optical density for up- and downwelling

This supplement complements Section 5.2.1 in the main text, by providing separate scatter plots and linear regressions for up- and downwelling actinic flux optical densities.

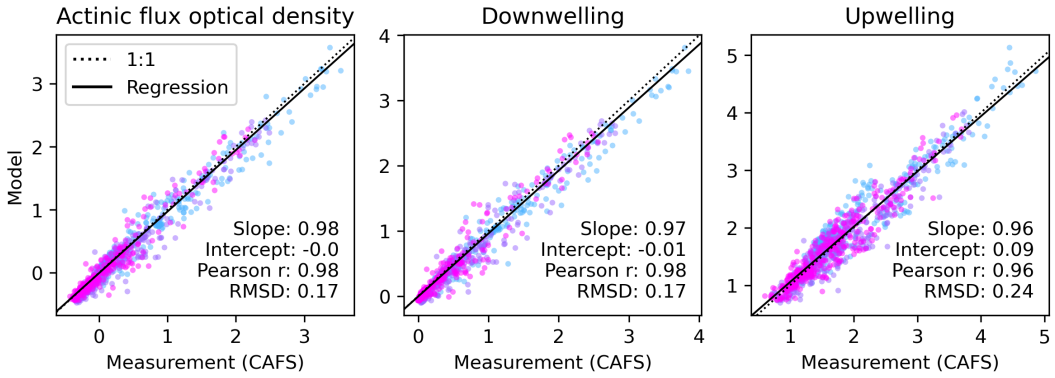

Figure S4. Correlation plots of measured (CAFS) and modeled (VPC) actinic flux optical density (AFOD, see Eq. 6). This figure is similar to Figure 8 in the main text. Datapoints in the plot are limited to the same wavelengths (340, 440 and 550 nm) as shown in Figure 5.

S5 Photolytic reactions

This section lists those reactions for which the photolysis frequency module in VPC can provide photolysis frequencies. Table S2 shows those reactions that are included in the original TUV photolysis frequency module and also covered by the spectral range of the CAFS instrument on board the FIREX-AQ aircraft. For these reactions, a model-measurement comparison as presented in Section 5.2.2 can be performed. The last four columns of the table show comparison results for the respective reaction: average observed photolysis frequencies ("Average") observed during the Shady fire flight, model-measurement linear regression results in terms of "Slope", "Intercept" and "Pearson R", as well as the root-mean-square of relative deviations ("RMSRD"). Table S3 lists the reactions that are included in the VPC photolysis frequency module but not considered for the comparison in the presented study. First two columns show reactions included in the TUV photolysis frequency module (from which the VPC photolysis frequency module was derived) but not covered by the spectral range of the CAFS instrument. The third column shows the 14 reactions by which we extended the standard TUV code. They are only included in the VPC photolysis frequency module.

Table S2. Reactions included in the original TUV photolysis frequency module and covered by the CAFS spectral range. Last four columns show results from the model-measurement comparison. See text for further details.

Reaction	Average	Slope	Intercept	Pearson R	RMSRD
$O_3 \rightarrow O_2 + O(^1D)$	8.77×10^{-06}	1.02	-3.87×10^{-07}	0.99	0.18
$NO_2 \rightarrow NO + O(^3P)$	6.56×10^{-03}	0.99	1.28×10^{-04}	0.98	0.14
$H_2O_2 \rightarrow 2\ OH$	3.84×10^{-06}	1.02	-2.69×10^{-09}	0.98	0.16
$NO_3 \rightarrow NO + O_2$	2.00×10^{-02}	1.04	5.27×10^{-05}	0.96	0.13
$NO_3 \rightarrow NO_2 + O(^3P)$	1.61×10^{-01}	1.00	1.22×10^{-03}	0.97	0.13
$N_2O_5 \rightarrow NO_3 + NO_2$	1.78×10^{-05}	1.02	-4.56×10^{-08}	0.98	0.16
$HNO_2 \rightarrow OH + NO$	1.03×10^{-03}	1.01	2.02×10^{-05}	0.98	0.15
$HNO_3 \rightarrow OH + NO_2$	2.23×10^{-07}	1.02	-5.11×10^{-09}	0.99	0.16
$HNO_4 \rightarrow HO_2 + NO_2$	3.16×10^{-06}	1.02	-3.27×10^{-08}	0.99	0.16
$CH_2O \rightarrow H + HCO$	1.61×10^{-05}	1.02	-1.29×10^{-07}	0.99	0.16
$CH_2O \rightarrow H_2 + CO$	3.07×10^{-05}	1.01	2.17×10^{-07}	0.98	0.16
$CH_3CHO \rightarrow CH_3 + HCO$	2.70×10^{-06}	1.02	-7.41×10^{-08}	0.99	0.16
$C_2H_5CHO \rightarrow C_2H_5 + HCO$	9.31×10^{-06}	1.02	-1.67×10^{-07}	0.99	0.16
$CH_3OOH \rightarrow CH_3O + OH$	2.98×10^{-06}	1.02	4.12×10^{-09}	0.98	0.16
$CH_3ONO_2 \rightarrow CH_3O + NO_2$	3.07×10^{-07}	1.02	-7.26×10^{-09}	0.99	0.16
$CH_3CH_2ONO_2 \rightarrow CH_3CH_2O + NO_2$	4.98×10^{-07}	1.02	-1.15×10^{-08}	0.99	0.16
$CH_3CO(OONO_2) \rightarrow CH_3CO(OO) + NO_2$	1.91×10^{-07}	1.02	-2.32×10^{-09}	0.99	0.16
$CH_3CO(OONO_2) \rightarrow CH_3CO(O) + NO_3$	8.20×10^{-08}	1.02	-9.94×10^{-10}	0.99	0.16
$CH_2{=}C(CH_3)CHO \rightarrow$ Products	3.15×10^{-06}	1.01	3.82×10^{-08}	0.98	0.16
$CH_3COCH{=}CH_2 \rightarrow$ Products	3.34×10^{-06}	1.02	3.53×10^{-09}	0.99	0.16
$CH_3COCH_3 \rightarrow CH_3CO + CH_3$	1.22×10^{-07}	1.01	-6.01×10^{-09}	0.99	0.21
$CH_3COCH_2CH_3 \rightarrow CH_3CO + CH_2CH_3$	2.55×10^{-06}	1.02	-5.44×10^{-08}	0.99	0.16
$CH_2(OH)COCH_3 \rightarrow CH_3CO + CH_2(OH)$	4.02×10^{-07}	1.02	-6.39×10^{-09}	0.99	0.16
$CH_2(OH)COCH_3 \rightarrow CH_2(OH)CO + CH_3$	4.02×10^{-07}	1.02	-6.39×10^{-09}	0.99	0.16
$CHOCHO \rightarrow HCO + HCO$	5.16×10^{-05}	0.99	7.66×10^{-07}	0.98	0.14
$CHOCHO \rightarrow H_2 + 2CO$	8.52×10^{-06}	1.02	-2.77×10^{-08}	0.98	0.16
$CHOCHO \rightarrow CH_2O + CO$	1.61×10^{-05}	1.02	-2.71×10^{-08}	0.98	0.15
$CH_3COCHO \rightarrow CH_3CO + HCO$	9.79×10^{-05}	1.01	1.66×10^{-06}	0.98	0.15
$CH_3COCOCH_3 \rightarrow$ Products	2.39×10^{-04}	0.96	4.60×10^{-06}	0.98	0.13
$Cl_2 \rightarrow Cl + Cl$	1.51×10^{-03}	1.00	1.94×10^{-05}	0.98	0.14
$ClO \rightarrow Cl + O(^3P)$	1.38×10^{-05}	1.02	-5.91×10^{-07}	0.99	0.17
$ClNO_2 \rightarrow Cl + NO_2$	1.84×10^{-04}	1.02	7.27×10^{-07}	0.98	0.16
$ClONO \rightarrow Cl + NO_2$	2.41×10^{-03}	1.01	1.65×10^{-05}	0.98	0.16
$ClONO_2 \rightarrow Cl + NO_3$	2.37×10^{-05}	1.00	2.37×10^{-07}	0.98	0.14
$ClONO_2 \rightarrow ClO + NO_2$	3.53×10^{-06}	1.02	-2.69×10^{-08}	0.99	0.16
$Br_2 \rightarrow Br + Br$	2.84×10^{-02}	0.96	4.73×10^{-04}	0.97	0.13
$BrO \rightarrow Br + O$	2.22×10^{-02}	1.01	2.27×10^{-04}	0.98	0.16
$HOBr \rightarrow OH + Br$	1.62×10^{-03}	0.99	2.33×10^{-05}	0.98	0.13
$BrNO \rightarrow Br + NO$	1.86×10^{-02}	0.98	2.56×10^{-04}	0.97	0.12
$BrONO \rightarrow Br + NO_2$	6.64×10^{-03}	1.01	4.97×10^{-05}	0.98	0.16
$BrONO \rightarrow BrO + NO$	6.64×10^{-03}	1.01	4.97×10^{-05}	0.98	0.16
$BrNO_2 \rightarrow Br + NO_2$	3.57×10^{-03}	0.98	6.58×10^{-05}	0.98	0.13
$BrONO_2 \rightarrow BrO + NO_2$	1.47×10^{-04}	0.99	1.94×10^{-06}	0.98	0.13
$BrONO_2 \rightarrow Br + NO_3$	8.36×10^{-04}	0.99	1.10×10^{-05}	0.98	0.13
$BrCl \rightarrow Br + Cl$	8.63×10^{-03}	0.97	1.48×10^{-04}	0.98	0.13
$CHBr_3 \rightarrow$ Products	3.95×10^{-07}	1.02	-8.99×10^{-09}	0.99	0.16

Table S3. List of photolytic reactions included in the VPC photolysis frequency module but not considered for the comparison in the presented study, as explained in the text.

Reactions included in original TUV module		Additional reactions
$O_2 \rightarrow O + O$	$O_3 \rightarrow O_2 + O(^3P)$	$OBrO \rightarrow BrO + O(^3P)$
$HO_2 \rightarrow OH + O$	$N_2O \rightarrow N_2 + O(^1D)$	$CH_2Br_2 \rightarrow CH_2Br + Br$
$N_2O_5 \rightarrow NO_3 + NO + O(^3P)$	NO_3-(aq) $\rightarrow NO_2$(aq) + O-	$CH_2Br_2 \rightarrow CH_2Br + Br$
NO_3-(aq) $\rightarrow NO_2$-(aq) + $O(^3P)$	$CH_3CHO \rightarrow CH_4 + CO$	$OIO \rightarrow I + O_2$
$CH_3CHO \rightarrow CH_3CO + H$	$HOCH_2OOH \rightarrow HOCH_2O. + OH$	$CH_3I \rightarrow CH_3 + I$
$CH_3(OONO_2) \rightarrow CH_3(OO) + NO_2$	$C_2H_5ONO_2 \rightarrow C_2H_5O + NO_2$	$CH_2I_2 \rightarrow CH_2I + I$
n-$C_3H_6ONO_2 \rightarrow C_3H_7O + NO_2$	1-$C_4H9ONO_2 \rightarrow$ 1-$C_4H9O + NO_2$	$CH_2ICl \rightarrow CH_2Cl + I$
2-$C_4H9ONO_2 \rightarrow$ 2-$C_4H9O + NO_2$	$CH_3CHONO_2CH_3 \rightarrow CH_3CHOCH_3 + NO_2$	$IONO_2 \rightarrow IO + NO_2$
$CH_2(OH)CH_2(ONO_2) \rightarrow CH_2(OH)CH_2(O.) + NO_2$	$CH_3COCH_2(ONO_2) \rightarrow CH_3COCH_2(O.) + NO_2$	$IONO_2 \rightarrow I + NO_3$
$C(CH_3)_3(ONO_2) \rightarrow C(CH_3)_3(O.) + NO_2$	$C(CH_3)_3(ONO) \rightarrow C(CH_3)_3(O) + NO$	$INO \rightarrow I + NO$
$CH_3CH_2CO(OONO_2) \rightarrow CH_3CH_2CO(OO) + NO_2$	$CH_3CH_2CO(OONO_2) \rightarrow CH_3CH_2CO(O) + NO_3$	$CH_3CH_2CH_2I \rightarrow$ Products
CH_2=CHCHO $\rightarrow$ Products	$HOCH_2CHO \rightarrow CH_2OH + HCO$	$INO_2 \rightarrow I + NO_2$
$HOCH_2CHO \rightarrow CH_3OH + CO$	$HOCH_2CHO \rightarrow CH_2CHO + OH$	$ICl \rightarrow I + Cl$
$CH_3COOH \rightarrow CH_3 + COOH$	$CH_3CO(OOH) \rightarrow$ Products	$IBr \rightarrow I + Br$
$CH_3COCO(OH) \rightarrow$ Products	$(CH_3)_2NNO \rightarrow$ Products	BALD $\rightarrow$ CHO + HO_2 + CO
$CF_2O \rightarrow$ Products	$ClO \rightarrow Cl + O(1D)$	
$ClOO \rightarrow$ Products	$OClO \rightarrow$ Products	
$ClOOCl \rightarrow Cl + ClOO$	$HCl \rightarrow H + Cl$	
$HOCl \rightarrow HO + Cl$	$NOCl \rightarrow NO + Cl$	
$CCl_4 \rightarrow Cl + CCl_3$	$CH_3OCl \rightarrow CH_3O + Cl$	
$CHCl_3 \rightarrow$ Products	$CH_3Cl \rightarrow Cl + CH_3$	
$CH_3CCl_3 \rightarrow CH_3CCl_2 + Cl$	$CCl_2O \rightarrow$ Products	
$CClFO \rightarrow$ Products	CCl_3F (CFC-11) $\rightarrow$ Products	
CCl_2F_2 (CFC-12) $\rightarrow$ Products	$CF_2ClCFCl_2$ (CFC-113) $\rightarrow$ Products	
CF_2ClCF_2Cl (CFC-114) $\rightarrow$ Products	CF_3CF_2Cl (CFC-115) $\rightarrow$ Products	
$CHClF_2$ (HCFC-22) $\rightarrow$ Products	CF_3CHCl_2 (HCFC-123) $\rightarrow$ Products	
CF_3CHFCl (HCFC-124) $\rightarrow$ Products	CH_3CFCl_2 (HCFC-141b) $\rightarrow$ Products	
CH_3CF_2Cl (HCFC-142b) $\rightarrow$ Products	$CF_3CF_2CHCl_2$ (HCFC-225ca) $\rightarrow$ Products	
CF_2ClCF_2CHFCl (HCFC-225cb) $\rightarrow$ Products	$CH_3Br \rightarrow CH_3 + Br$	
CF_2Br_2 (Halon-1202) $\rightarrow$ Products	CF_2BrCl (Halon-1211) $\rightarrow$ Products	
CF_3Br (Halon-1301) $\rightarrow$ Products	CF_2BrCF_2Br (Halon-2402) $\rightarrow$ Products	
$I_2 \rightarrow I + I$	$IO \rightarrow I + O$	
$HOI \rightarrow I + OH$	Perfluoro 1-Iodopropane $\rightarrow$ Products	

S6 Overview plots for all transects

Overview plots of all 20 investigated plume transects, as a complement to the material in Section 5.1. Descriptions of Figures 5 in the main text apply.

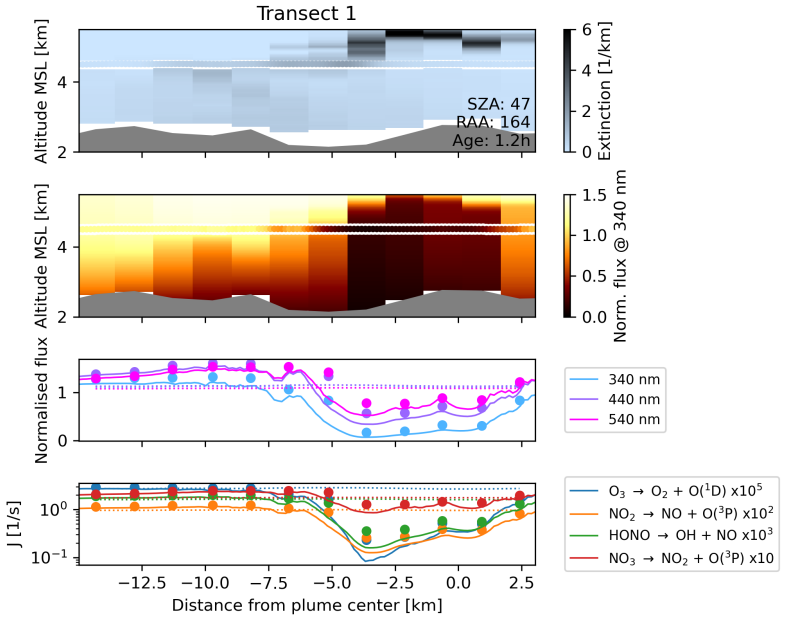

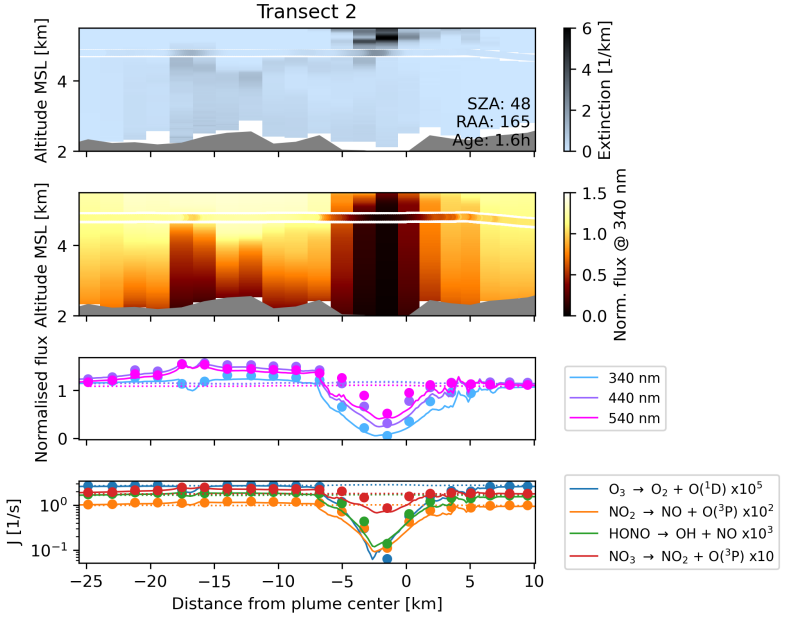

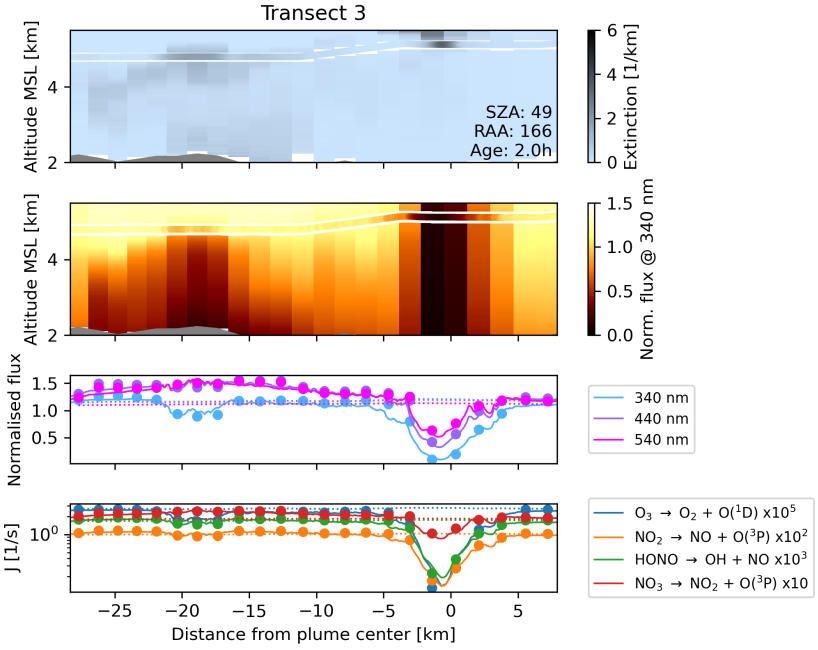
Transect 3
Altitude MSL [km]
SZA: 49
RAA: 166
Age: 2.0h
Extinction [1/km]
Norm. flux @ 340 nm
Normalised flux
340 nm
440 nm
540 nm
J [1/s]
$O_3 \rightarrow O_2 + O(^1D)$ x10^5
$NO_2 \rightarrow NO + O(^3P)$ x10^2
HONO → OH + NO x10^3
$NO_3 \rightarrow NO_2 + O(^3P)$ x10
Distance from plume center [km]

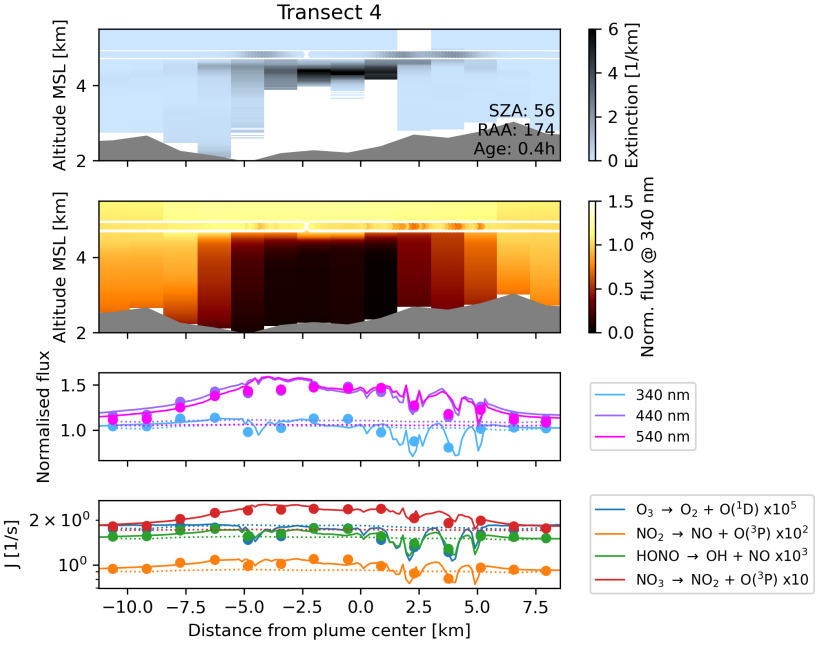
Transect 4
Altitude MSL [km]
SZA: 56
RAA: 174
Age: 0.4h
Extinction [1/km]
Norm. flux @ 340 nm
Normalised flux
340 nm
440 nm
540 nm
J [1/s]
$O_3 \rightarrow O_2 + O(^1D)$ x10^5
$NO_2 \rightarrow NO + O(^3P)$ x10^2
HONO → OH + NO x10^3
$NO_3 \rightarrow NO_2 + O(^3P)$ x10
Distance from plume center [km]

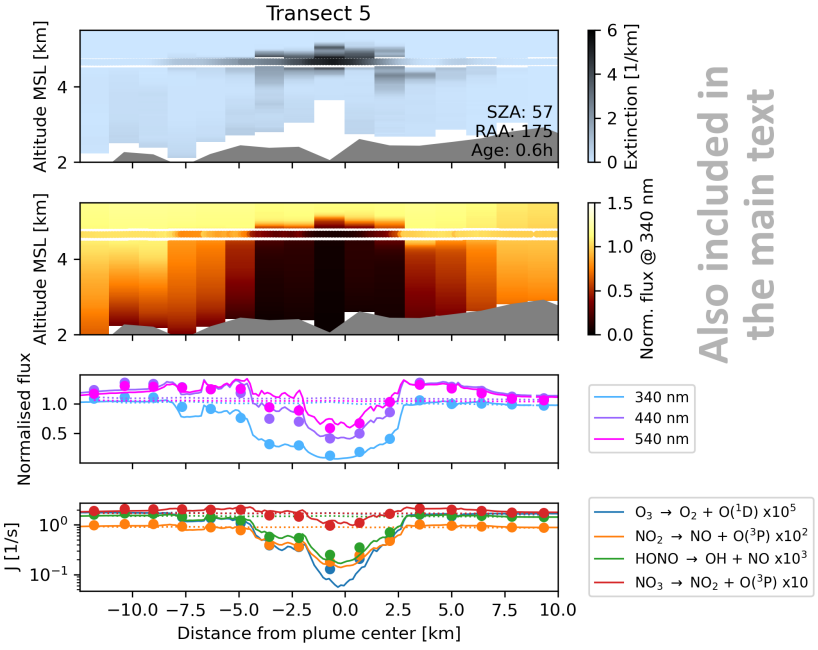

Also included in the main text

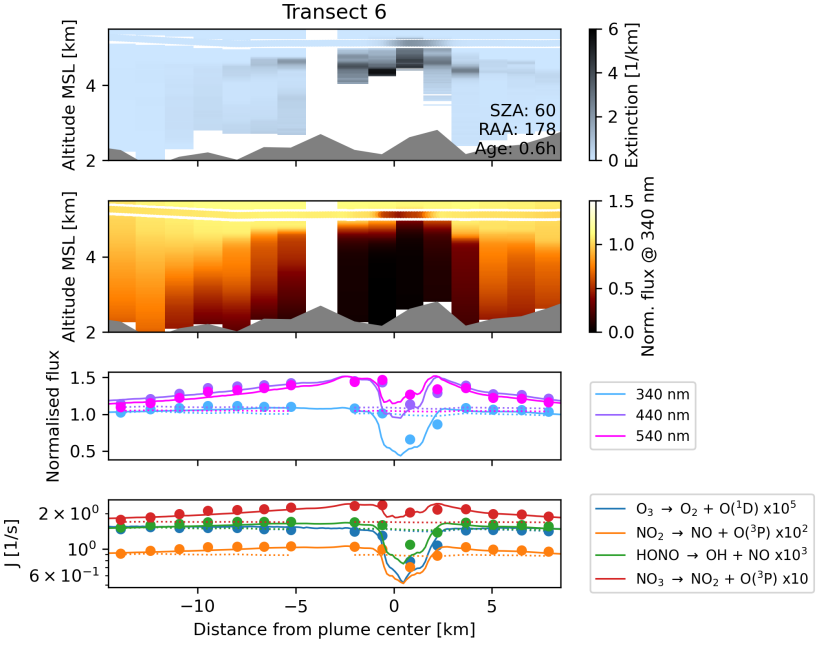

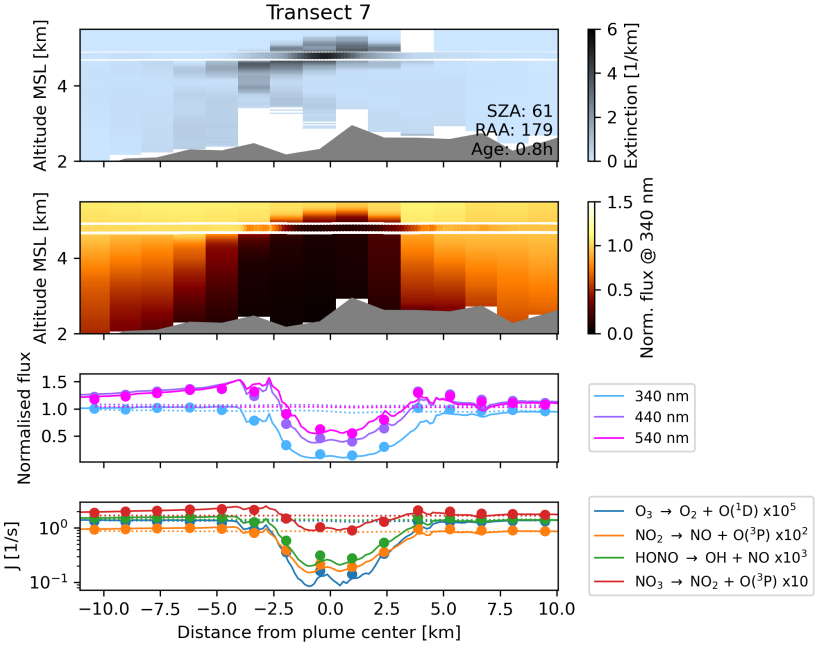

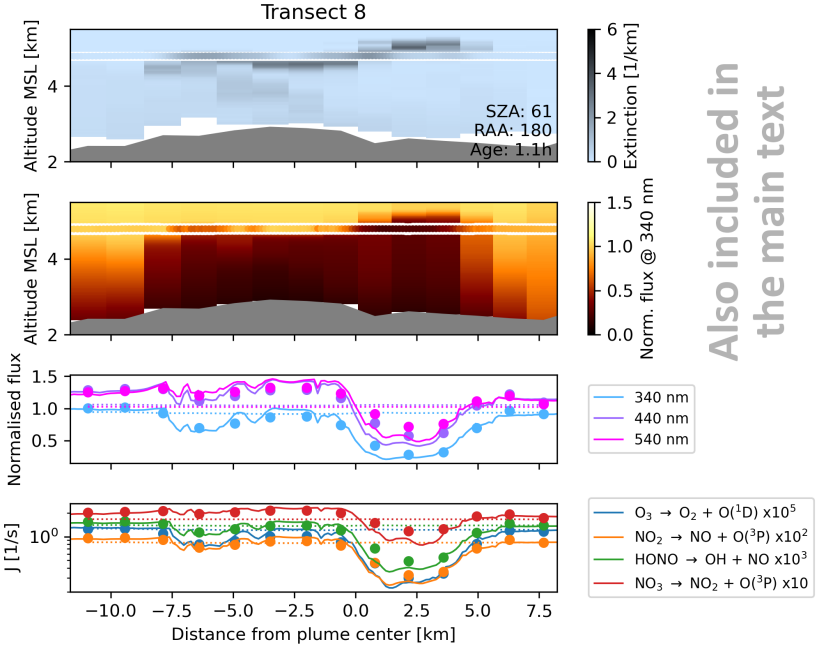

Also included in the main text

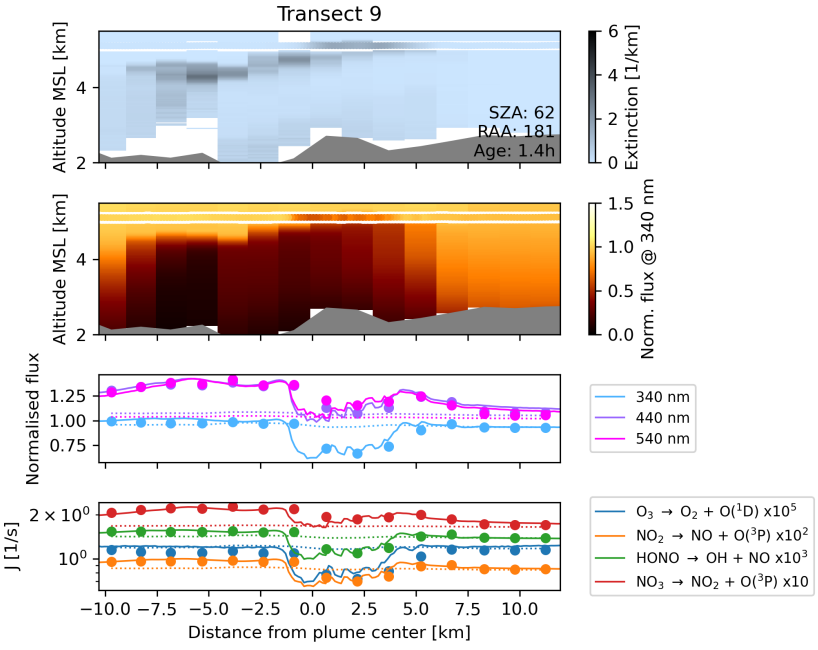
Transect 9
Altitude MSL [km]
SZA: 62
RAA: 181
Age: 1.4h
Extinction [1/km]
Norm. flux @ 340 nm
Normalised flux
340 nm
440 nm
540 nm
J [1/s]
O3 → O2 + O(1D) x10^5
NO2 → NO + O(3P) x10^2
HONO → OH + NO x10^3
NO3 → NO2 + O(3P) x10
Distance from plume center [km]

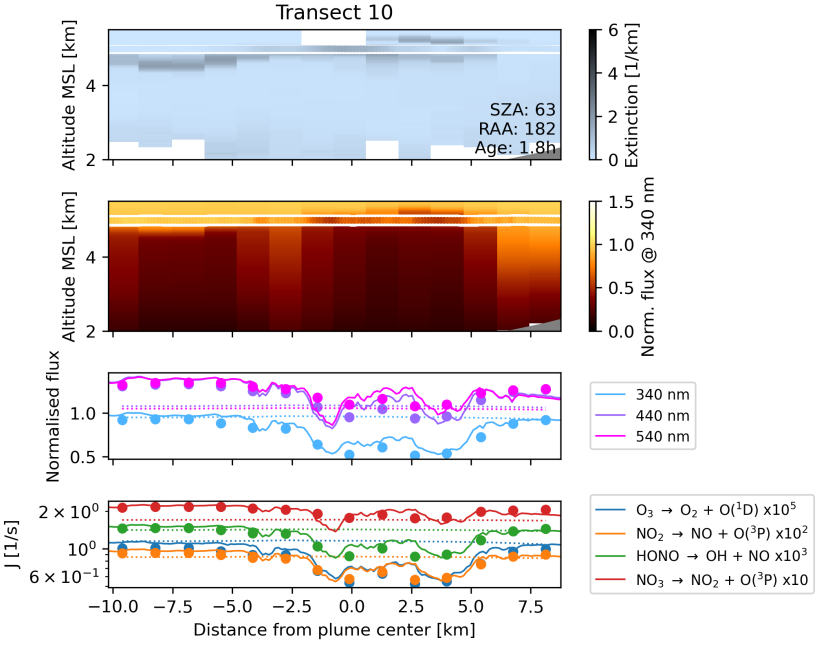
Transect 10
Altitude MSL [km]
SZA: 63
RAA: 182
Age: 1.8h
Extinction [1/km]
Norm. flux @ 340 nm
Normalised flux
340 nm
440 nm
540 nm
J [1/s]
O3 → O2 + O(1D) x10^5
NO2 → NO + O(3P) x10^2
HONO → OH + NO x10^3
NO3 → NO2 + O(3P) x10
Distance from plume center [km]

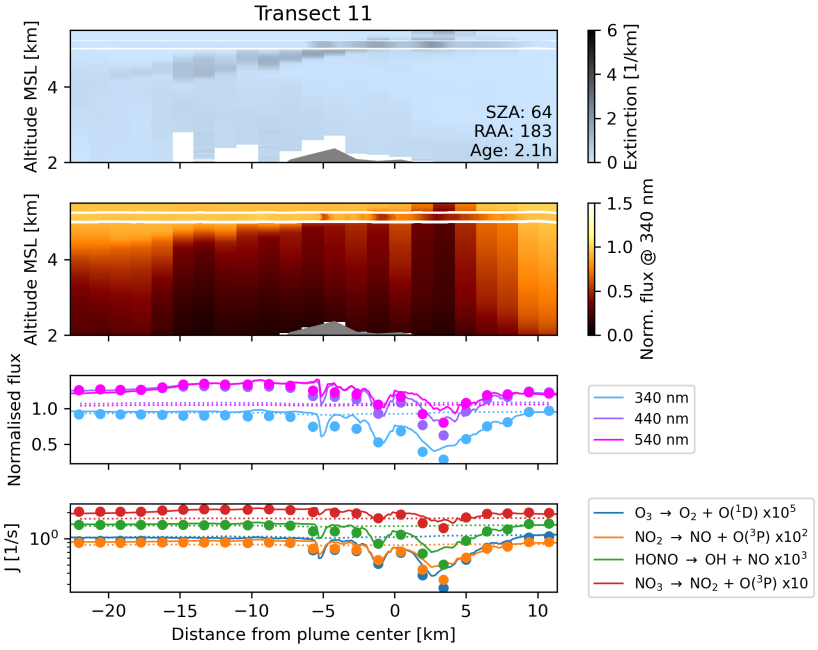
Transect 11
Altitude MSL [km]
SZA: 64
RAA: 183
Age: 2.1h
Extinction [1/km]
Norm. flux @ 340 nm
Normalised flux
340 nm
440 nm
540 nm
J [1/s]
$O_3 \rightarrow O_2 + O(^1D)$ x10^5
$NO_2 \rightarrow NO + O(^3P)$ x10^2
HONO → OH + NO x10^3
$NO_3 \rightarrow NO_2 + O(^3P)$ x10
Distance from plume center [km]

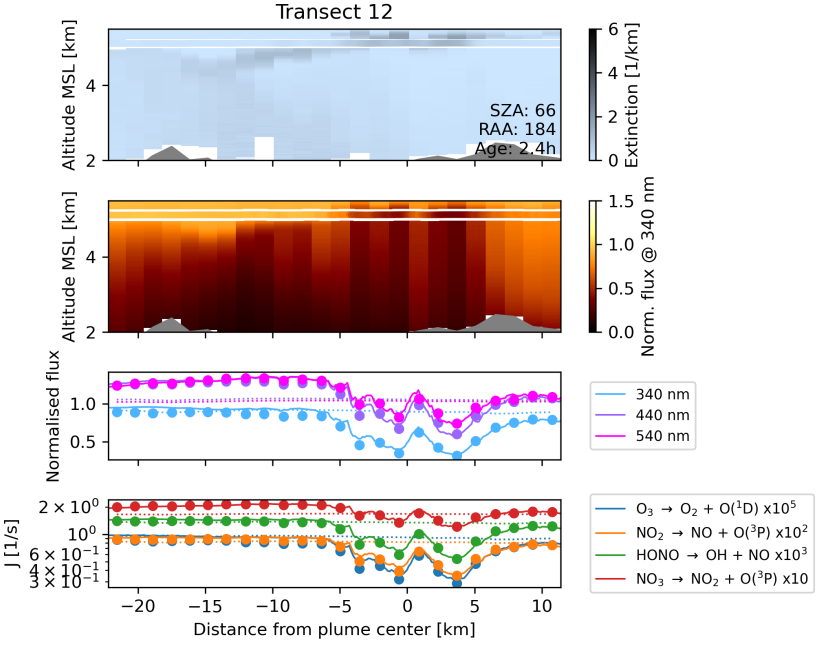
Transect 12
Altitude MSL [km]
SZA: 66
RAA: 184
Age: 2.4h
Extinction [1/km]
Norm. flux @ 340 nm
Normalised flux
340 nm
440 nm
540 nm
J [1/s]
$O_3 \rightarrow O_2 + O(^1D)$ x10^5
$NO_2 \rightarrow NO + O(^3P)$ x10^2
HONO → OH + NO x10^3
$NO_3 \rightarrow NO_2 + O(^3P)$ x10
Distance from plume center [km]

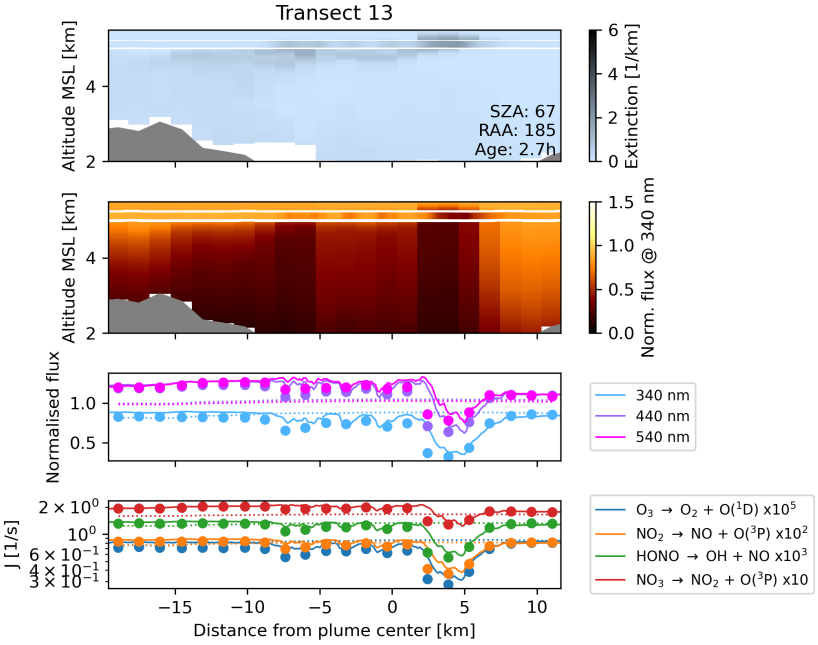

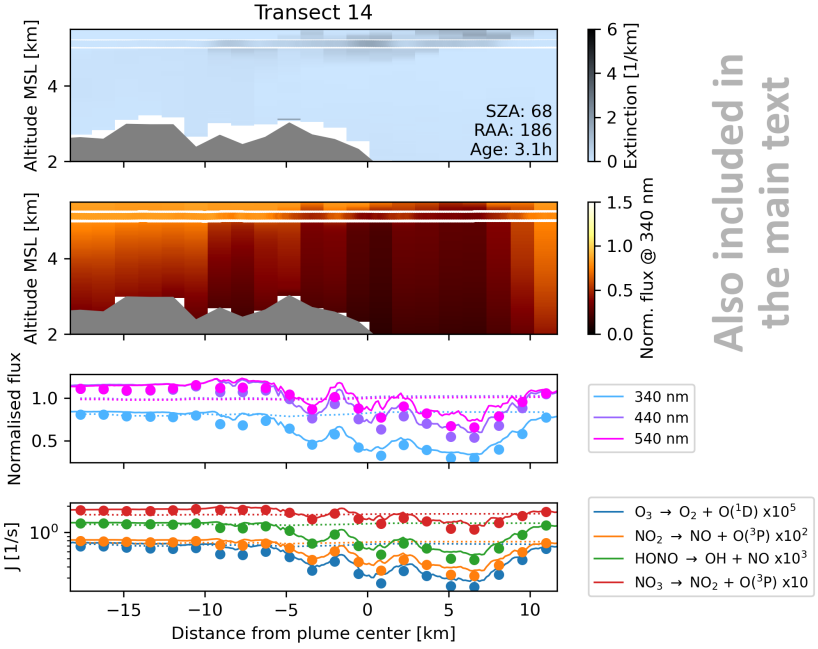

Also included in the main text

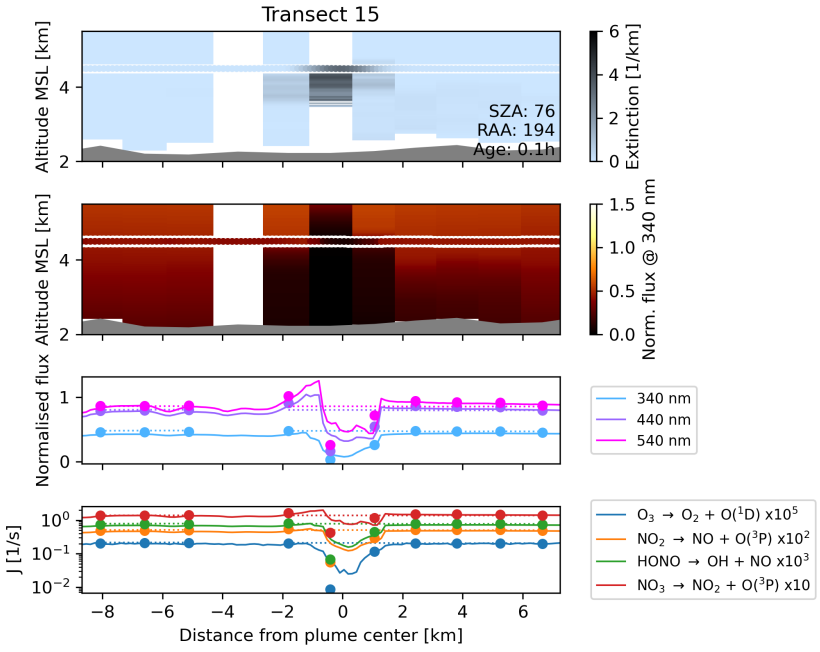
Transect 15
Altitude MSL [km]
SZA: 76
RAA: 194
Age: 0.1h
Extinction [1/km]
Norm. flux @ 340 nm
Normalised flux
340 nm
440 nm
540 nm
J [1/s]
$O_3 \rightarrow O_2 + O(^1D)$ x10^5
$NO_2 \rightarrow NO + O(^3P)$ x10^2
HONO → OH + NO x10^3
$NO_3 \rightarrow NO_2 + O(^3P)$ x10
Distance from plume center [km]

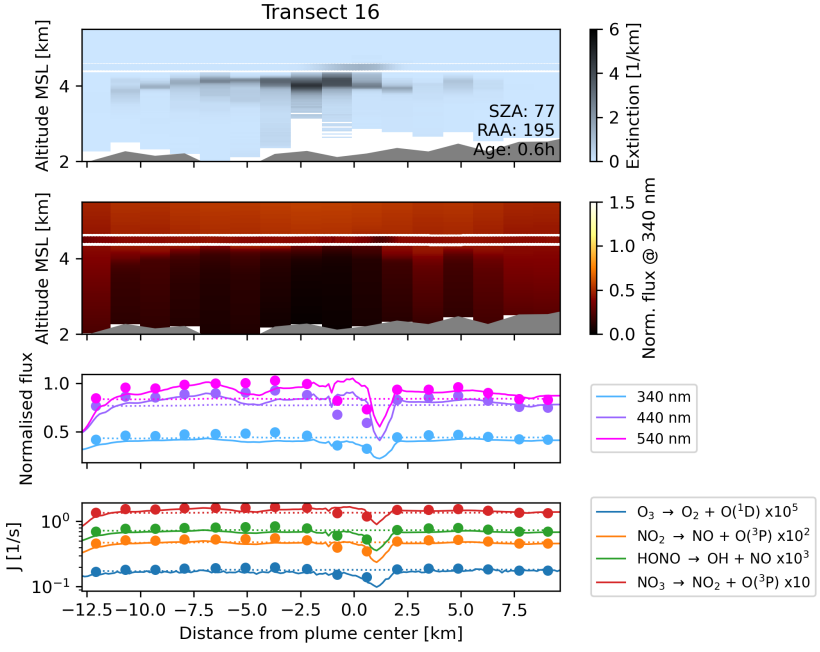
Transect 16
Altitude MSL [km]
SZA: 77
RAA: 195
Age: 0.6h
Extinction [1/km]
Norm. flux @ 340 nm
Normalised flux
340 nm
440 nm
540 nm
J [1/s]
$O_3 \rightarrow O_2 + O(^1D)$ x10^5
$NO_2 \rightarrow NO + O(^3P)$ x10^2
HONO → OH + NO x10^3
$NO_3 \rightarrow NO_2 + O(^3P)$ x10
Distance from plume center [km]

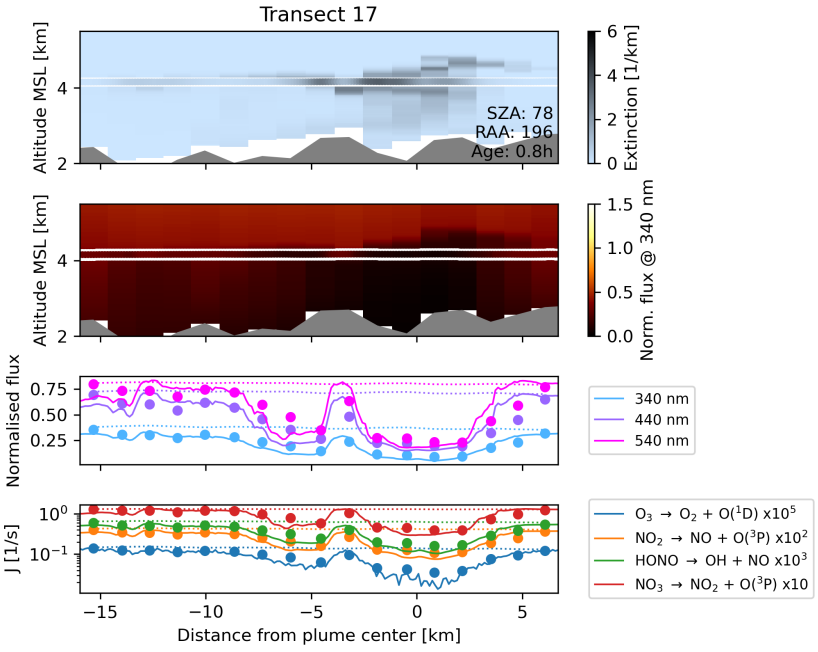
Transect 17
Altitude MSL [km]
SZA: 78
RAA: 196
Age: 0.8h
Extinction [1/km]
Norm. flux @ 340 nm
Normalised flux
340 nm
440 nm
540 nm
J [1/s]
$O_3 \rightarrow O_2 + O(^1D)$ x10^5
$NO_2 \rightarrow NO + O(^3P)$ x10^2
HONO → OH + NO x10^3
$NO_3 \rightarrow NO_2 + O(^3P)$ x10
Distance from plume center [km]

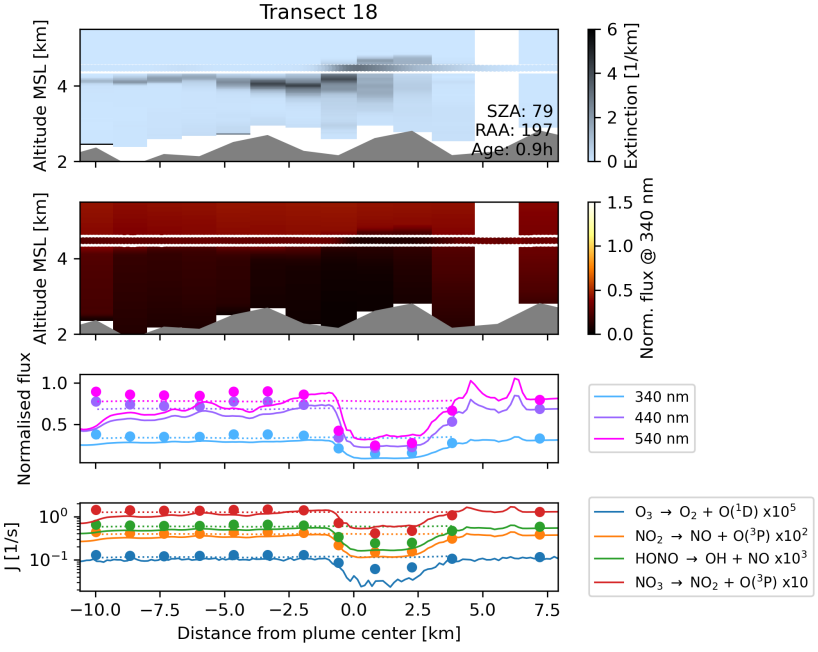
Transect 18
Altitude MSL [km]
SZA: 79
RAA: 197
Age: 0.9h
Extinction [1/km]
Norm. flux @ 340 nm
Normalised flux
340 nm
440 nm
540 nm
J [1/s]
$O_3 \rightarrow O_2 + O(^1D)$ x10^5
$NO_2 \rightarrow NO + O(^3P)$ x10^2
HONO → OH + NO x10^3
$NO_3 \rightarrow NO_2 + O(^3P)$ x10
Distance from plume center [km]

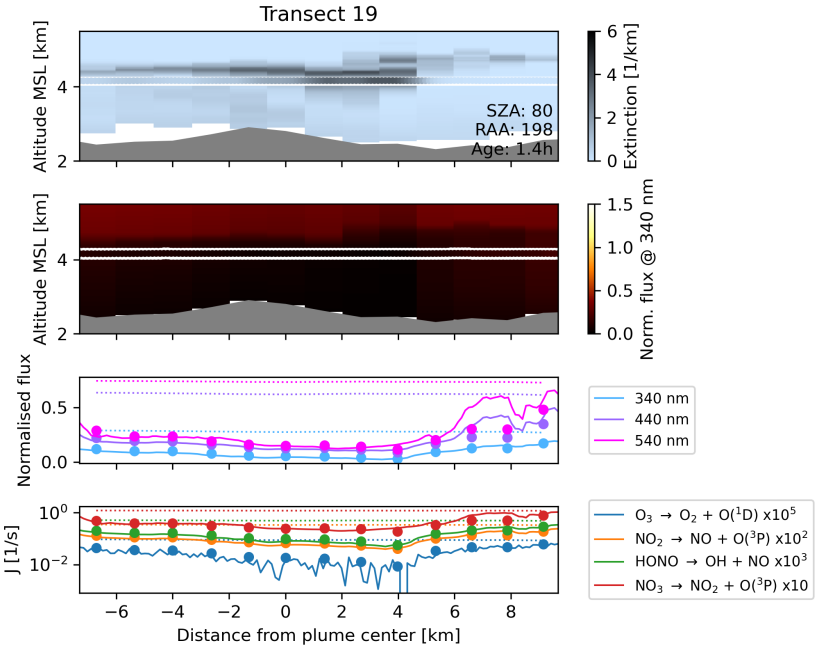

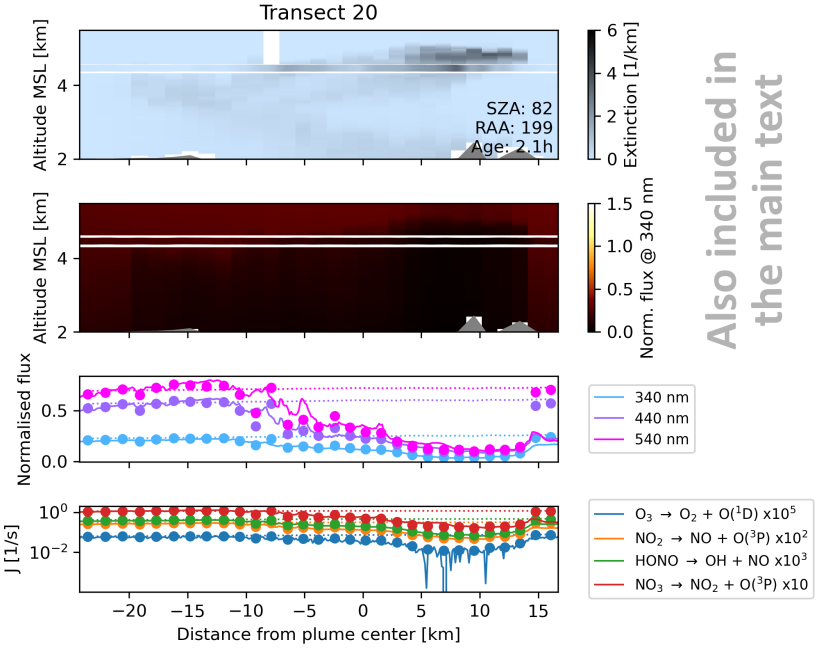

Also included in the main text